Gridded Hourly Precipitation Analysis from High-Density Rain Gauge Network over the Yangtze–Huai Rivers Basin during the 2007 Mei-Yu Season and Comparison with CMORPH

YALI LUO

State Key Laboratory of Severe Weather, Chinese Academy of Meteorological Sciences, Beijing, China

WEIMIAO QIAN

Shijiazhuang Meteorological Bureau, Shijiazhuang, China

RENHE ZHANG

State Key Laboratory of Severe Weather, Chinese Academy of Meteorological Sciences, Beijing, China

DA-LIN ZHANG

State Key Laboratory of Severe Weather, Chinese Academy of Meteorological Sciences, Beijing, China, and Department of Atmospheric and Oceanic Science, University of Maryland, College Park, College Park, Maryland

(Manuscript received 6 September 2012, in final form 2 April 2013)

ABSTRACT

Heavy rainfall hit the Yangtze–Huai Rivers basin (YHRB) of east China several times during the prolonged 2007 mei-yu season, causing the worst flood since 1954. There has been an urgent need for attaining and processing high-quality, kilometer-scale, hourly rainfall data in order to understand the mei-yu precipitation processes, especially at the mesoβ and smaller scales. In this paper, the authors describe the construction of the 0.07°-resolution gridded hourly rainfall analysis over the YHRB region during the 2007 mei-yu season that is based on surface reports at 555 national and 6572 regional automated weather stations with an average resolution of about 7 km. The gridded hourly analysis is obtained using a modified Cressman-type objective analysis after applying strict quality control, including not only the commonly used internal temporal and spatial consistency and extreme value checks, but also verifications against mosaic radar reflectivity data. This analysis reveals many convectively generated finescale precipitation structures that could not be seen from the national station reports. A comprehensive quantitative assessment ensures the quality of the gridded hourly precipitation data. A comparison of this dataset with the U.S. Climate Prediction Center morphing technique (CMORPH) dataset on the same resolution suggests the dependence of the latter's performance on different rainfall intensity categories, with substantial underestimation of the magnitude and width of the mei-yu rainband as well as the nocturnal and morning peak rainfall amounts, due mainly to its underestimating the occurrences of heavy rainfall (i.e., $>10\,\mathrm{mm\,h^{-1}}$).

1. Introduction

Climatologically, the mei-yu season over the Yangtze–Huai Rivers basin (YHRB; Fig. 1b) in east-central China from mid-June to mid-July is one of the three heavy rainfall periods in China. The other two are the early summer rainy season from mid-May to mid-June over south China and the summer rainy season in north-northeast China after mid-July (e.g., Ding 1992). This intraseasonal variation exhibits sharp northward shifts among the three regions, which are associated with rapid intraseasonal changes in large-scale circulations over East Asia (e.g., Ueda and Yasunari 1996; Ding and Chan 2005). The large-scale circulations and mesoscale convective systems (MCSs) associated with the mei-yu–frontal

Corresponding author address: Dr. Yali Luo, State Key Laboratory of Severe Weather, Chinese Academy of Meteorological Sciences, Beijing 100081, China.
E-mail: yali@cams.cma.gov.cn; yali_luo@hotmail.com

DOI: 10.1175/JHM-D-12-0133.1

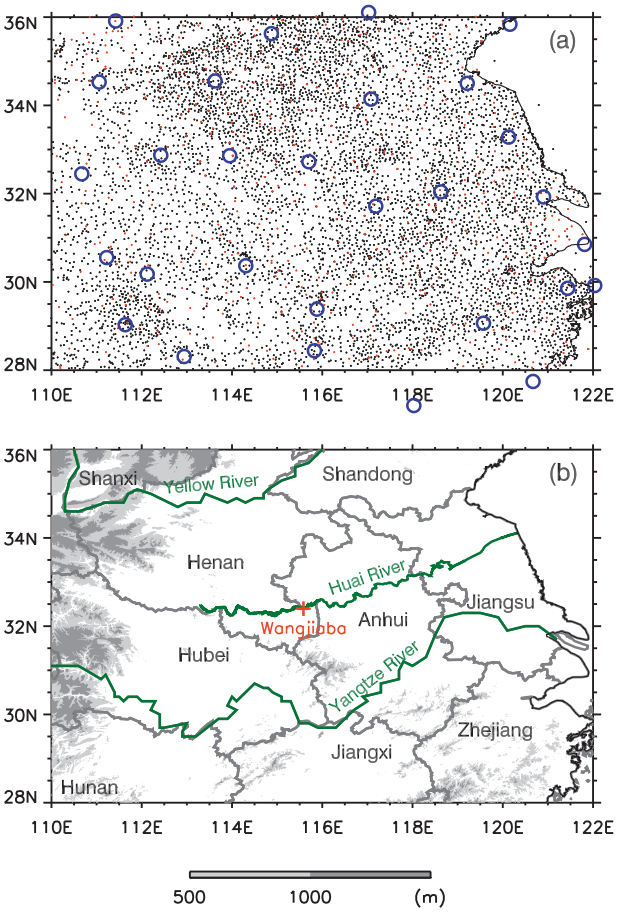

FIG. 1. (a) Distribution of the rain gauges [national stations (red dots); regional stations (black dots)] and the weather radars (blue circles) within the analysis domain. (b) Names and borders of the provinces stationed around the analysis domain, along with Yangtze, Huai, and Yellow rivers (green lines) and the location of Wangjiaba reservoir (red cross). Shadings represent terrain heights.

rainfall have been extensively studied during the past decades (see Ni and Zhou 2006). Recently, mesoscale and convective-scale processes involved in the mei-yu–frontal heavy precipitation have been investigated through cloud-resolving simulations with the horizontal grid spacing of kilometer (e.g., Luo et al. 2010) and subkilometer scales (Zhang and Zhang 2012). Indeed, these ultrahigh-resolution modeling studies provided much new insight into the initiation and subsequent evolution of deep convection with a hierarchy of rainfall structures at different horizontal scales.

However, there has been the lack of such high-resolution precipitation observations to reveal detailed spatial and temporal distributions of the mei-yu precipitation in east China, and similarly for heavy precipitating MCSs occurring elsewhere around the world. Clearly, such high-resolution data are much needed to aid in the understanding of complicated precipitation processes and the verification of satellite precipitation products and numerical weather prediction (NWP) models. Recently, the National Meteorological Information Center (NMIC) of the China Meteorological Administration (CMA) started providing the 0.1°-resolution gridded hourly precipitation product across China from 2008 onward (Pan et al. 2012). This product is developed using the optimum interpolation technique by combining the CMA's hourly rain gauge network data with a satellite-retrieved precipitation product of the National Oceanic and Atmospheric Administration (NOAA), namely, the NOAA Climate Prediction Center's morphing technique (CMORPH) dataset (Joyce et al. 2004). The latter is generated on an 8-km resolution over the globe (i.e., 60°S–60°N) with 30-min temporal resolution beginning in December 2002; more technical details may be found at www.cpc.noaa.gov/products/janowiak/cmorph_description.html. However, the CMORPH satellite precipitation product tends to underestimate substantially the early morning peaks of the mei-yu rainfall (Shen et al. 2010).

The mei-yu season could also undergo substantial interannual variations (Luo et al. 2013). The year of 2007 is well known in China because heavy rainfall during the mei-yu season generated the worst flood in the Huai River valley since 1954 (Tao et al. 2008), causing tremendous economic losses and leaving more than 10 million people homeless. On 9 July, the water level of the Wangjiaba reservoir (see Fig. 1b for the location) was up to 29.3 m, which exceeded the reservoir warning level by 1.8 m and prompted the Chinese Ministry of Water Resources to make a sluice in the reservoir. Therefore, there has been an urgent need for processing high-quality, kilometer-scale, hourly precipitation data over the YHRB during the 2007 mei-yu season in order to study the precipitation processes at the mesoβ and smaller scales (Zhao et al. 2007), as well as to evaluate satellite precipitation products and NWP models. This urgent need motivated the present study.

By the end of 2009, CMA implemented approximately 30 000 automated weather stations (AWSs) across China, where hourly precipitation is measured by siphon or tipping-bucket rain gauges and recorded automatically. A majority of these stations are operated at the regional level, and about 2000 stations are operated at the national level, where hourly precipitation reports go through a manual quality check. There are 555 national stations and 6572 regional stations located over the YHRB region (28°–36°N, 110°–122°E; see Fig. 1a). The average resolution between the stations (including both national and regional) over the YHRB is about 7 km, which is

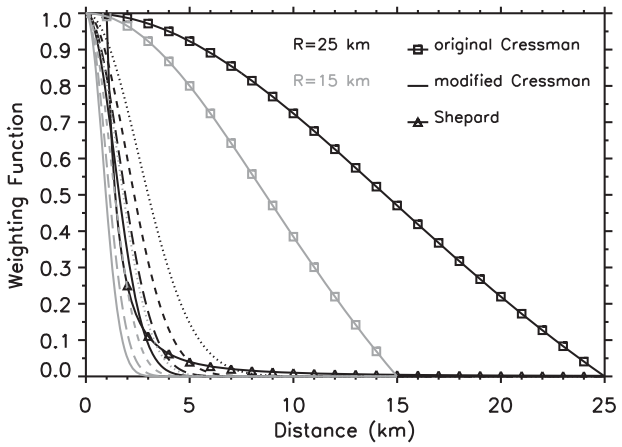

FIG. 2. Weighting functions for the original Cressman (solid lines with squares), modified Cressman (lines without symbols), and the Shepard (solid line with triangles) as a function of distance. For the original Cressman and modified Cressman, weighting functions with an influence radius of 25 km and 15 km, respectively, are represented by lines in black and gray. Weighting functions for the modified Cressman also vary with rainfall intensity: $>40\,\text{mm h}^{-1}$ (solid lines), 20–40 mm h^{-1} (long dashed lines), 5–20 mm h^{-1} (short dashed lines), and 0.1–5 mm h^{-1} (dotted lines).

approximately 4 times higher than that between the national stations (i.e., 26 km).

The objectives of this study are to 1) describe the procedures to obtain the high-quality, kilometer-scale, hourly rainfall analysis over the YHRB region for the 2007 mei-yu season; 2) demonstrate the high quality of this analysis by both comprehensive quantitative assessments and showing finescale characteristics of precipitation with selected cases; and 3) evaluate the quality of the CMORPH data by comparing it with our gridded analysis. To achieve the above objectives, considerable effort has been made to collect the digitalized hourly precipitation reports from nine provincial meteorological bureaus that are stationed around the YHRB region (Fig. 1b). The next section describes the quality control to these reports, followed by the gridded analysis of the quality-controlled station reports in section 3. Section 4 presents the assessment of the gridded hourly rainfall data, while section 5 compares it to the CMORPH data. A summary of this study and possible applications of this analysis data will be given in the final section.

2. Quality control of the AWS rainfall reports

A quality-control procedure is used to flag and remove bad rainfall reports. This is achieved through not only the commonly used temporal and spatial consistency and extreme value checks, but also verifications against mosaic radar reflectivity observations. A detailed description of the mosaic reflectivity data is given in the appendix. The quality-control procedure, applied to the hourly rainfall reports, consists of three components. First, the horizontal distribution of hourly precipitation rates at the AWSs is visually compared hour by hour to that of the mosaic reflectivity data at 3-km altitude. There are typically 9–10 snapshots of the mosaic reflectivity during each hour because the ground radars complete each volume scan in about 6 min. Obvious inconsistencies between the two data sources are occasionally detected, suggesting suspicious rainfall reports. For example, there are times when the hourly rainfall reports indicate large rainfall amounts at isolated AWSs, whereas the weather radar did not detect any echo aloft during the hour. Second, the extreme value check is conducted, with an upper limit of 140 mm h^{-1}, following the suggestion from the NMIC of CMA (Ren et al. 2010). Finally, a temporal and spatial consistency check is applied to further determine whether a suspicious report is a bad one. A bad report of hourly rainfall at a station is replaced with an estimated rainfall amount, which is carefully determined in accordance with concurrent rainfall reports at nearby stations (located within 20 km from the target station) and/or hourly rainfall reports at the same station in 3 h before/after the hour. In the end, about 0.03% of the station rainfall reports are corrected. All of these problematic reports are from the regional stations.

3. Gridded analysis of the AWS rainfall reports

Based on the quality-controlled station reports, a gridded hourly rainfall dataset is generated using a modified Cressman interpolation method (Cressman 1959). The rainfall analysis is generated on the same grid resolution as CMORPH (8 km × 8 km), which is close to the average distance of the AWSs. About 77% of the grid boxes contain at least one AWS. Rainfall amount at grid point (i, j) P_{ij} is estimated as

$$P_{ij} = \frac{\sum_{k=1}^{N} W_{ijk} \times P_k}{\sum_{k=1}^{N} W_{ijk}}, \tag{1}$$

where W_{ijk} is the weighting factor from station k and P_k is the rainfall report at station k. The Cressman weighting function W at any grid point (i, j) from station k can be represented as

$$W = \begin{cases} \dfrac{(R^2 - r^2)}{(R^2 + r^2)} & r \le R \\ 0 & r > R \end{cases}, \tag{2}$$

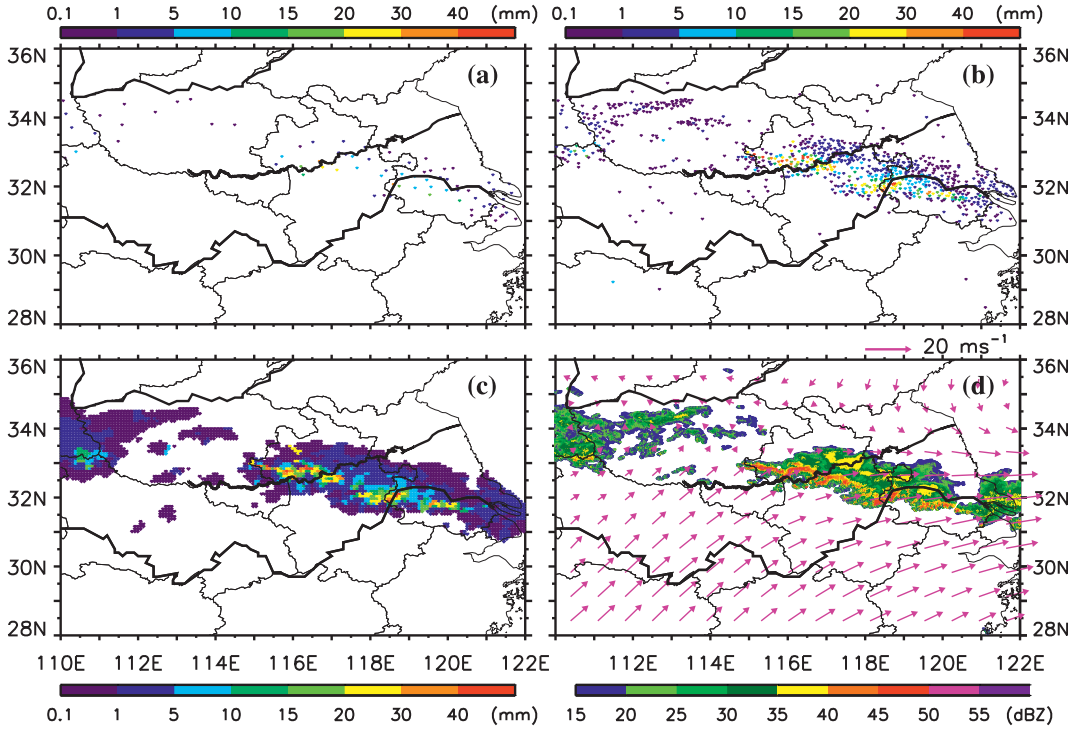

FIG. 3. Hourly rainfall rates ending at 0100 UTC 8 Jul 2007 from (a) observations at the national stations, (b) observations at both national and regional stations, and (c) gridded analysis. (d) A snapshot of radar reflectivity (shaded in dBZ) at 3-km altitude at 0030 UTC 8 Jul 2007, superimposed by the 700-hPa flow vectors at 0000 UTC 8 July 2007.

where r is the distance between the station and the grid point and R is the influence radius. To retain the local centers of intense rainfall, W is modified to be

$$W = \begin{cases} \left[\dfrac{(R^2 - r^2)}{(R^2 + r^2)}\right]^{(2+a)\times(6+2a)} & r \le R \\ 0 & r > R \end{cases}, \qquad (3)$$

where a equals 1, 2, 3, or 4 corresponding to four grades of precipitation intensity: [0.1, 5], (5, 20], (20, 40], and >40 mm h^{-1}, respectively. Moreover, R varies with the station density near the grid point in this study. To determine an optimum influence radius, experiments are conducted with the value of R increasing from 8 to 13 km. Visual inspection of horizontal distributions of the gridded rainfall, station rainfall, and radar reflectivity suggests generally good performance of the gridded analysis with $R \sim 13$ km. Therefore, the default (minimum) value of R is set to 13 km. It is required in the gridded analysis that at least six stations are located within the radius R from the grid point of concern. About 85% of the R values are less than 25 km.

The weighting functions for the original Cressman and the modified Cressman with R of 15 and 25 km, respectively, and those for the Shepard (1986) method are shown in Fig. 2. Both the modified Cressman and the Shepard weighting functions decrease much more rapidly with distance than the original Cressman weighting functions, suggesting smaller impacts from remote points for the former two methods. The modified Cressman weighting functions decrease with distance even faster for intense precipitation than lighter precipitation. As will be shown in the following section, this gridded analysis with the modified Cressman weighting function effectively retains the localized heavy rainfall centers, which is consistent with the finding of Zhang et al. (2009).

4. Assessment of the gridded rainfall product

a. Qualitative examination

Horizontal distributions of the gridded hourly rainfall data have been visually verified against the corresponding station rainfall reports and mosaic radar reflectivity at 3-km altitude. Results show high quality of the gridded data in terms of hourly rainfall pattern and amount, including rainfall extremes. An example is given in Fig. 3, showing the distribution of hourly rainfall ending at 0100 UTC 8 July 2007 (Figs. 3a–c) along with a snapshot

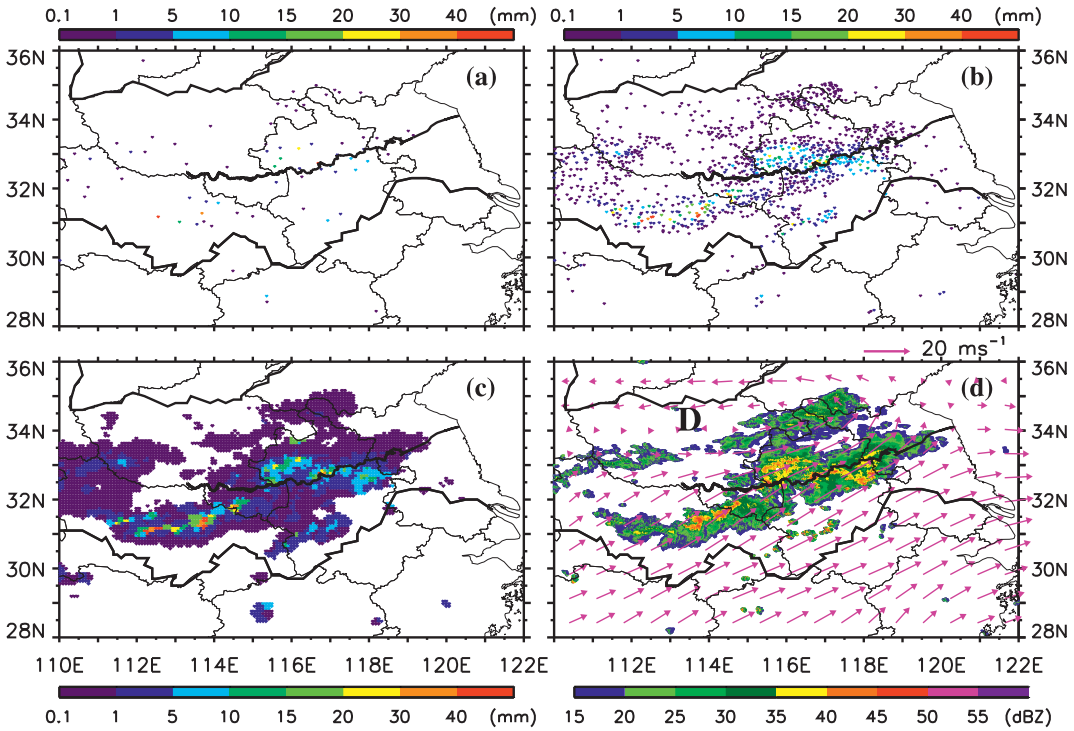

FIG. 4. (a)–(c) As in Figs. 3a–c, but for 1200 UTC 8 Jul 2007. (d) Radar reflectivity (shaded in dBZ) at 3-km altitude at 1130 UTC 8 Jul 2007, superimposed by the 700-hPa flow vectors at 1200 UTC 8 July 2007.

of radar reflectivity at 0030 UTC and horizontal winds on 700 hPa at 0000 UTC 8 July 2007 (Fig. 3d). The radar reflectivity pattern suggests the presence of multiple contiguous MCSs, each consisting of a west-northwest–east-southeast oriented leading convective line (>40 dBZ) and an elongated stratiform precipitation region trailing to the northeast. This mei-yu–frontal precipitation occurred at the northern edge of the warm and moist southwesterly monsoonal flow. While the entire precipitation region extended several hundreds of kilometers from west to east, the widths of the convective and stratiform raining regions at the surface were only about 10 and 100–200 km, respectively. The national station reports alone (Fig. 3a) missed even some convective–stratiform rainfall structures and, more significantly, many finescale structures that may be important for detailed studies of the mei-yu–frontal MCS. In contrast, the gridded analysis (Fig. 3c) is able to capture these features, including the distribution of many local rainfall centers and rainbands along the mei-yu–frontal MCS.

Figure 4 presents another example at about 1200 UTC 8 July 2007, when the mei-yu–frontal precipitation over the YHRB was modulated by a low-level subsynoptic-scale vortex centered at (113.5°E, 34°N) interacting with the southwesterly monsoonal flow (Fig. 4d). The radar reflectivity observations suggest that the precipitation, that is, convective rain embedded within broader-stratiform rainy regions, was located mainly in the southeastern quadrant of the vortex. There were two bands of intense precipitation in Anhui, Henan, and Hubei Provinces: one oriented from west to east along the Huai River and the other extended from the eastern Hubei northeastward to the southeastern Henan. New convective cells formed in south Anhui within the warm and moist southwesterly monsoonal flow. These precipitation features of various scales are clearly represented by the gridded analysis (Fig. 4c). However, they can hardly be seen from the national station rainfall reports (Fig. 4a).

TABLE 1. Summary of cross-validation tests for the rain gauge–based analyses of hourly precipitation over the YHRB for the mei-yu seasons of 2007 (19 Jun to 26 Jul), 2008 (8 Jun to 24 Jul), and 2009 (1 Jul to 1 Aug). Determination of starting and ending dates of the mei-yu season is described in detail by Luo et al. (2013).

Statistics	2007	2008	2009
Bias (mm)	−0.01	−0.01	0.00
Mean absolute error (mm)	0.31	0.21	0.20
RMS error (mm)	1.72	1.44	1.43
Correlation coefficient	0.65	0.59	0.62
Relative standard deviation	0.89	0.89	0.87

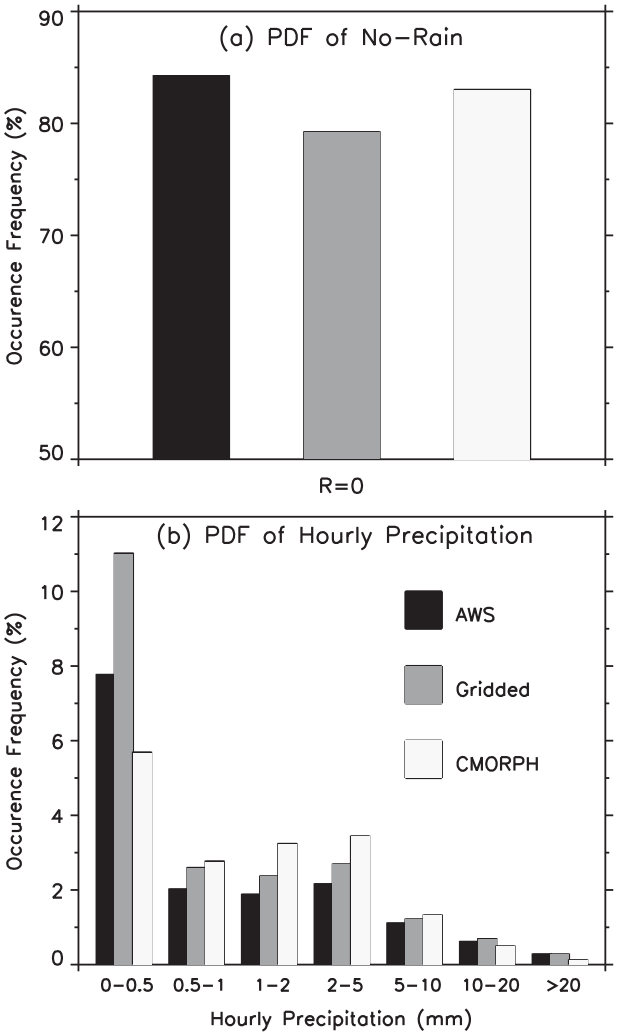

FIG. 5. PDF (%) of hourly precipitation amounts (mm h^{-1}) defined by the rain gauge station reports (black bars), the rain gauge–based gridded analysis (gray bars), and CMORPH (light gray bars) at all stations over the YHRB during the 2007 mei-yu season.

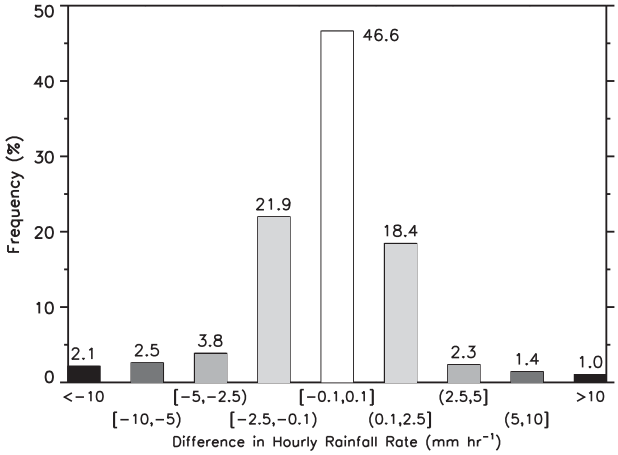

FIG. 6. Occurrence frequency of the differences in hourly rainfall rate (mm h^{-1}) between the gridded analysis from the regional station reports (rain_g) and the national station reports (rain_o), that is, rain_g minus rain_o, over the YHRB during the 2007 mei-yu season.

We may state, based on our visual examination, with high confidence that the newly constructed gridded analysis data capture well the hourly, fine spatial distribution of many rainfall events during the 2007 mei-yu season. Thus, we have decided to release these valuable gridded analysis data in the hope of getting them the widest possible applications; the dataset can now be accessed via http://cadata.cams.cma.gov.cn/news2/upload/2012_07/gridded_hourly_rainfall.zip. In the next two subsections, we will provide a variety of quantitative assessments on the quality of the gridded rainfall dataset.

b. *Cross-validation tests*

Cross-validation tests are conducted, using the method of Chen et al. (2008), to quantify the performance of the gridded analysis technique in interpolating hourly precipitation. Ten percent of the stations were randomly selected from the entire databases of N (=7127) stations over the YHRB region. Hourly precipitation reports from these stations are withdrawn, and the rain gauge observations for the remaining 90% of stations are used to define the analyzed values at the locations of the withdrawn stations. This process is repeated 10 times so that each station is withdrawn once. Visual inspection of the 10 sets of withdrawn stations shows relatively homogeneous distributions. The analyzed values at the station locations are then compared to the corresponding withdrawn station observations to assess the quantitative accuracy of the interpolated hourly precipitation field. An alternative validation method (see Hu et al. 2008) is also tested. That is, one of the stations is selected and an hourly precipitation report for this station is withdrawn. The rain gauge observations for the remaining 7126 stations are used to produce a gridded dataset, which is then interpolated to the location of the withdrawn station and compared with the corresponding withdrawn station observation. This process is repeated 7127 times. Results from the two sets of tests are nearly identical, and therefore, only results from the first method are shown in this section.

Table 1 shows the statistics of the cross-validation tests that are calculated from the analyzed hourly precipitation values and the quality-controlled hourly observations station by station for the mei-yu season of not only 2007, but also 2008 and 2009. Results show that the biases (−0.01, −0.01, and 0.00 mm) are close to zero, the mean absolute errors (0.31, 0.21, and 0.20 mm) are very small, and the root-mean-square (RMS) errors (1.72,

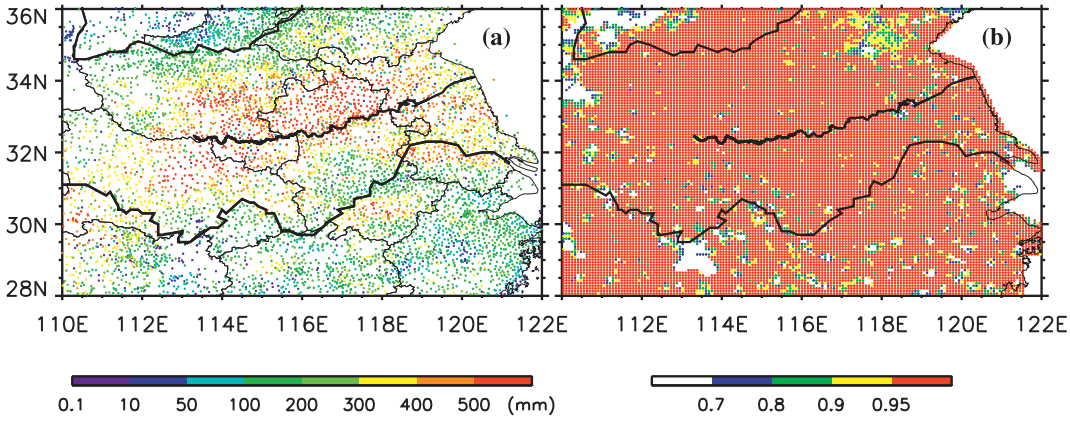

FIG. 7. (a) Total rainfall amount (mm) accumulated at the national and regional stations during the mei-yu season of 2007 (from 0000 UTC 19 June to 0000 UTC 27 July 2007). (b) Correlation between two gridded hourly rainfall datasets: one based on reports from both the national and regional stations and the other based on reports from the regional stations only. Also shown are the three major rivers (thick lines) and provincial borders and coastlines (thin lines).

1.44, and 1.43 mm) are also small. The correlation coefficients (0.65, 0.59, and 0.62) and the ratios of standard deviation (analysis divided by observed; 0.89, 0.89, and 0.87) are reasonably large. These statistics suggest that the analyzed hourly precipitation fields represent reasonably well the magnitude, spatial distribution, and temporal evolution of the observations. Moreover, the consistency obtained for the three years suggests that the analysis methodology is robust and that the statistics calculated in this study are stable.

A probability density function (PDF), or histogram, of the hourly precipitation amount is an important statistic of precipitation fields. Figure 5 shows PDFs for the observed and analyzed hourly precipitation amounts at all stations (solid and gray bars). An examination of the precipitation intensity histograms enables us to, at least qualitatively, judge how well the relative intensity of precipitation is reproduced by the analyzed fields. The observational histogram is largely dominated by no-rain events (with the frequency of occurrence of ~84%). The greater the precipitation rate, the lower is the frequency of occurrence. About 1.98% of the total precipitation rate is greater than 5 mm h^{-1}. The analyzed field captures these features in the observational histogram: the no-rain frequency is ~80%, while the precipitation frequency of greater than 5 mm h^{-1} is 2.16%. A major difference is that the analyzed field contains slightly more occurrences of light rainfall, that is, (0.0, 5) mm h^{-1}, and slightly fewer occurrences of clear sky than the observations.

c. *Validation of the gridded analysis based on regional AWS reports*

To further assess the quality of the gridded hourly rainfall dataset, we generate another gridded hourly rainfall dataset based on the quality-controlled rainfall reports at the regional stations only, that is, reports from the national stations are withdrawn on purpose (hereafter referred to as R-only gridding). The quality of this gridded dataset is assessed by comparing its rainfall amounts at the grid points that are the closest to the national stations with the corresponding observations. Since manual quality checks at the national stations have been constructed in nearly real time by weather observers, rainfall reports at these stations are treated herein as the ground truth. A histogram of the differences between the R-only gridding and the national station observations, given in Fig. 6, shows close agreements: approximately 47% of the differences are better than ± 0.1 mm h^{-1}, 87% are better than ± 2.5 mm h^{-1}, and only about 3% exceed 10 mm h^{-1}.

Moreover, the correlation coefficient C between the R-only gridding and the all-station gridding is calculated for each grid point (over land). Horizontal distribution of the correlation coefficients is shown in Fig. 7b, whereas the accumulated total rainfall amount over all the stations during the entire 2007 mei-yu season is given in Fig. 7a. Clearly, correlations are high at most locations within the analysis domain: C is greater than or equal to 0.9 over 80% of the grid points. Only 1.9% of the grid points have C less than 0.5, where the station density is relatively coarse and the rainfall amount is relatively small. Significance tests suggest that the correlations are significant at a 0.01 level for all of the grids. These results further corroborate the high quality of the gridded hourly rainfall dataset based on the quality-controlled reports from all the stations.

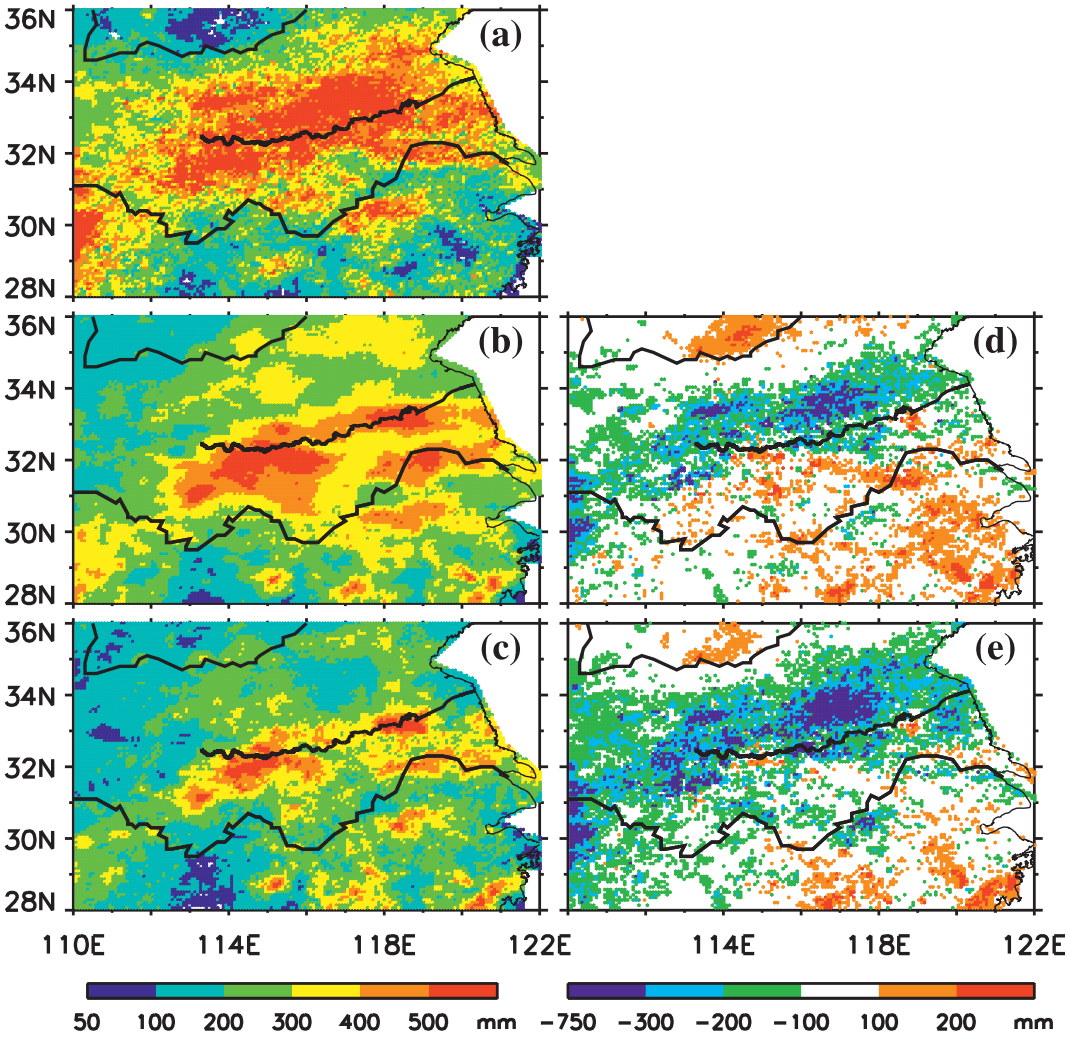

FIG. 8. Total rainfall amount (mm) accumulated over the YHRB during the mei-yu season of 2007 that is derived from (a) the gauge-based analysis and (b) CMORPH, and (c) MWCOMB. (d),(e) Differences between (b) and (a) [CMORPH minus gauge-based analysis], and between (c) and (a) [MWCOMB minus gauge-based analysis], respectively. Also shown are the three major rivers (thick lines) and coastlines (thin lines).

5. Comparison between the gauge-based analysis and CMORPH

In this section, we examine the performance of CMORPH (Joyce et al. 2004) using our gridded hourly rainfall analysis both on the same grid resolution. CMORPH and five satellite estimates have been compared to a gauge-based analysis on a 0.25° latitude–longitude grid over China during the 3-yr period of 2005–07, at 3-hourly or daily intervals (Shen et al. 2010). Results show that CMORPH exhibits better performance in depicting the spatial pattern and temporal variations of precipitation relative to the other five satellite estimates. However, all satellite products substantially underestimated the early morning peak of the mei-yu rainfall over central-eastern China (Shen et al. 2010); this rainfall peak is an important characteristic of the mei-yu rainfall, as mentioned in section 1. Although the previous studies have used the rain gauge analysis to verify the satellite-based precipitation estimates over East Asia (e.g., Xie et al. 2007; Shen et al. 2010), we herein make the first effort to examine CMORPH at its original spatial resolution (8 km) and close to its original time resolution (hourly). To better understand effects of the morphing processing, we have also included in the comparison the microwave combined (MWCOMB) data, which are simple averages of several microwave-derived precipitation estimates but without any propagation or morphing of the related features (Joyce et al. 2004).

a. Rainfall accumulation

Figure 8 shows the spatial distributions of rainfall accumulation during the 2007 mei-yu season from our

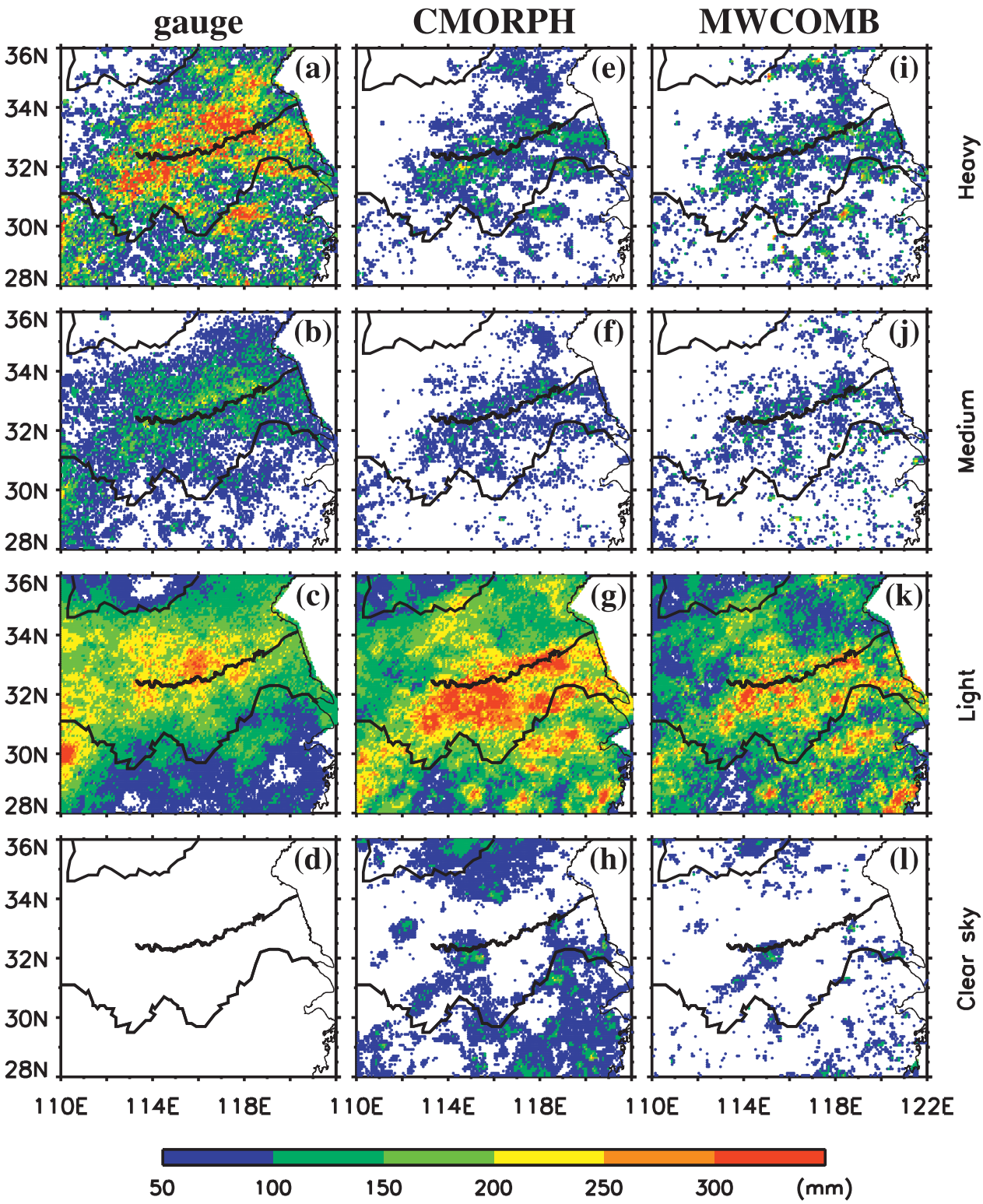

FIG. 9. Rainfall accumulation over the YHRB during the mei-yu season of 2007 derived from (a)–(d) the rain gauge–based analysis and (e)–(h) the CMORPH. (i)–(l) Differences in the rainfall accumulation between the CMORPH and the rain gauge–based analysis. The hourly rainfall rates are categorized into four groups (from top to bottom) when the gauge-based rainfall analysis indicates occurrences of heavy ($>10\,\mathrm{mm\,h^{-1}}$), medium (5–$10\,\mathrm{mm\,h^{-1}}$), and light (0.1–$5\,\mathrm{mm\,h^{-1}}$) rainfall, and clear sky ($<0.1\,\mathrm{mm\,h^{-1}}$) categories.

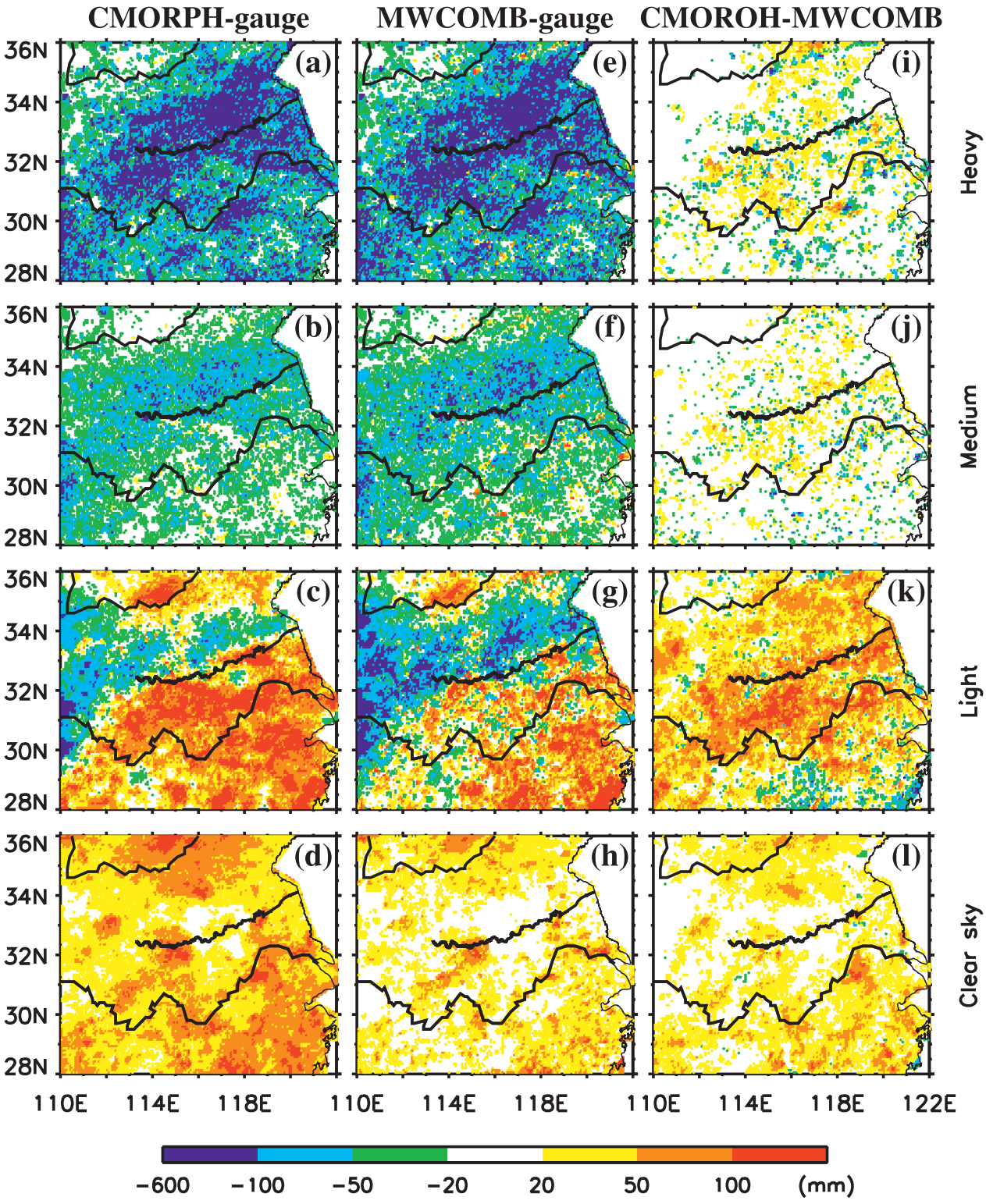

FIG. 10. The differenced rainfall accumulations between (a)–(d) CMORPH and the rain gauge–based analysis, (e)–(h) MWCOMB and the rain gauge–based analysis, and (i)–(l) CMORPH and MWCOMB. The hourly rainfall rates are categorized into four groups (from top to bottom) when the gauge-based rainfall analysis indicates occurrences of heavy (>10 mm h^{-1}), medium (5–10 mm h^{-1}), and light (0.1–5 mm h^{-1}) rainfall, and clear sky (<0.1 mm h^{-1}) categories.

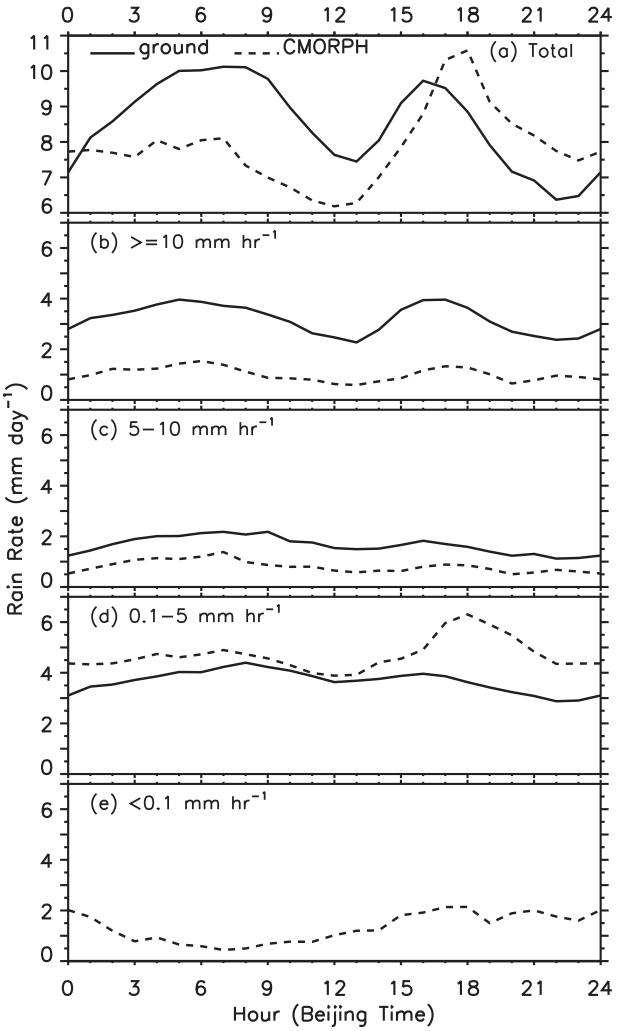

FIG. 11. Diurnal cycle of precipitation rates (mm day^{-1}) averaged over the YHRB during the 2007 mei-yu season derived from the rain gauge–based analysis (solid) and CMORPH (dashed) for (a) total rainfall rates and different rainfall intensity categories based on the gauge-based analysis: (b) >10 mm h^{-1}, (c) 5–10 mm h^{-1}, (d) 0.1–5 mm h^{-1}, and (e) <0.1 mm h^{-1}.

hourly gauge analysis, CMORPH, MWCOMB, and the differences (i.e., the two satellite precipitation estimates minus the gauge-based analysis). A major feature of the rainfall accumulation from the rain gauge observations (Fig. 8a) is a west–east oriented rainband of greater than 400 mm over the Huai River basin. This feature is to some extent captured by CMORPH (Fig. 8b) and MWCOMB (Fig. 8c). However, CMORPH and MWCOMB tend to underestimate rainfall amounts, and thus, the rainband appears too narrow relative to that in the rain gauge observations. On the other hand, CMORPH and MWCOMB overestimate the rainfall accumulation outside of the major rainband, that is, to the south of Huai River and east of 114°E and near the northern edge of the analysis region where the total accumulative rainfall amount is relatively small. Compared to MWCOMB, CMORPH provides larger amounts of the accumulated rainfall over the analysis region. Therefore, the underestimation of intensity and spatial extension of the mei-yu rainband seems to be lessened by CMORPH, but the overestimation of rainfall amounts outside of the gauge-observed major rainfall centers appears to be worse from CMORPH, relative to MWCOMB.

Rainfall accumulation from a variety of rainfall intensities based on the rain gauge–based analysis—heavy (>10 mm h^{-1}), medium (5–10 mm h^{-1}), light (0.1–5 mm h^{-1}), and clear sky (<0.1 mm h^{-1})—are inspected (Fig. 9). The results suggest that the performances of CMORPH and MWCOMB under each rainfall category (Figs. 9i–l) are qualitatively similar (Figs. 9e–h), but quantitative differences are substantial, especially for the light rainfall and clear sky categories. Both CMORPH and MWCOMB significantly underestimate the heavy rainfall (cf. Figs. 9a,e,i), and they also underestimate the medium rainfall (cf. Figs. 9b,f,j), albeit to a lesser extent. Note that the CMORPH's underestimation of heavy rainfall could also be clearly seen from the PDFs of hourly precipitation amount at the AWSs (Fig. 5b). On the other hand, CMORPH and MWCOMB overestimate the rainfall accumulation when the rain gauge–based analysis indicates light rainfall (cf. Figs. 9c,g,k) or clear sky categories (cf. Figs. 9d,h,l), leading to the overestimation of the total accumulative rainfall outside of the major centers (Figs. 8d,e). Moreover, for the light rainfall category, the performance of CMORPH and MWCOMB is more complicated than for the other three rainfall categories. While they generally overestimate the surface rainfall over the analysis region, an underestimation is seen from the Huai River northward to about 35° or 34°N (MWCOMB or CMORPH) and near the western edge of the analysis region. Differences in accumulative rainfall among the three datasets are shown in Fig. 10 for each rainfall category based on the gauge analysis, confirming the conclusions drawn from Fig. 9. The most significant difference between CMORPH and MWCOMB is that CMORPH produces larger accumulative rainfall amounts for the light rainfall and clear sky categories than MWCOMB (Figs. 10i–l), suggesting a spatial-smoothing impact caused by the morphing processing.

b. Diurnal variation of precipitation

Diurnal cycles of the mei-yu precipitation derived from the rain gauge–based analysis and CMORPH are given in Fig. 11. For the total rainfall rates (Fig. 11a), the gauge-based analysis exhibits a bimodal distribution,

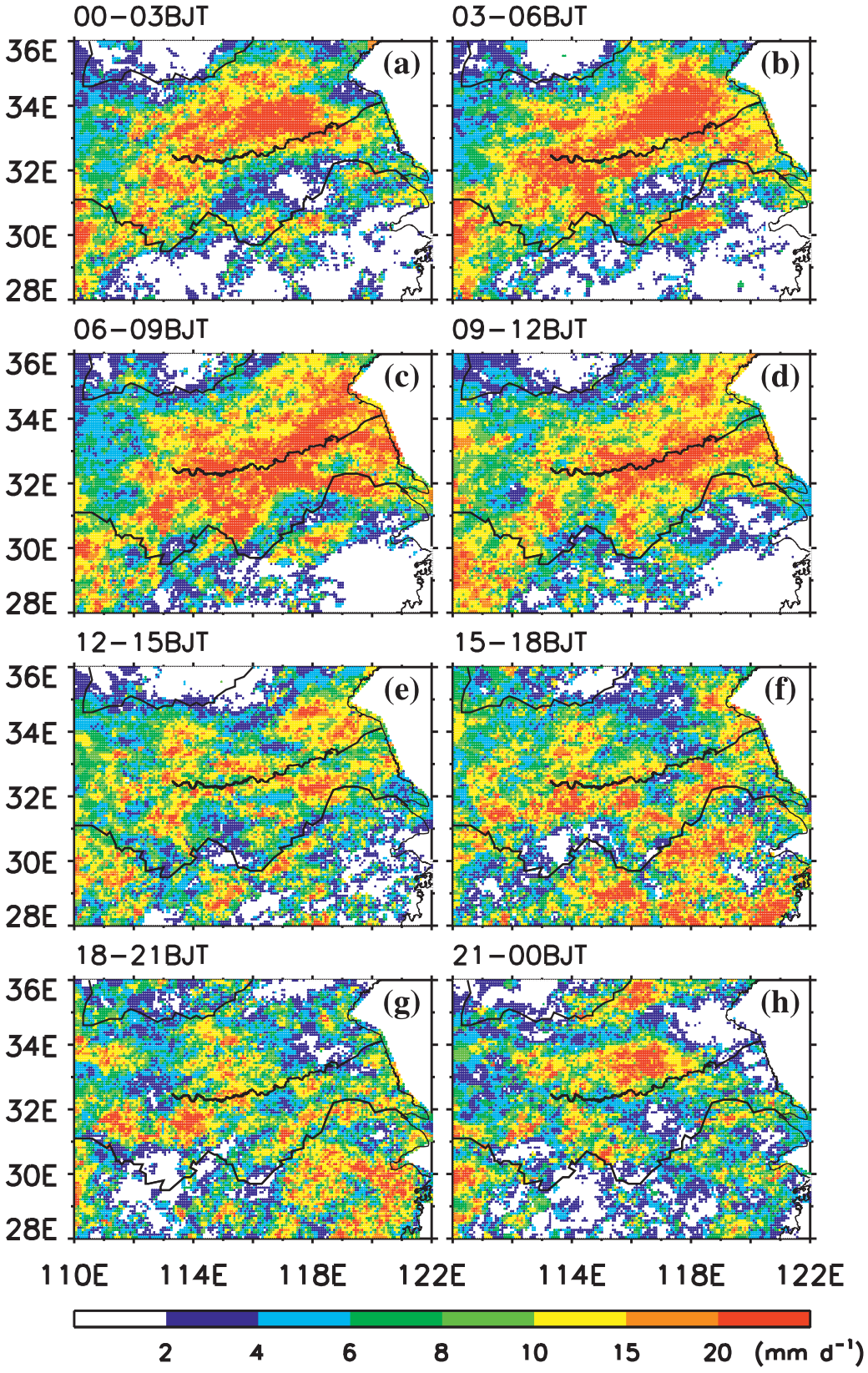

FIG. 12. Rainfall rates distribution from the rain gauge–based analysis (mm day^{-1}) averaged over each 3-h daily during the 2007 mei-yu period.

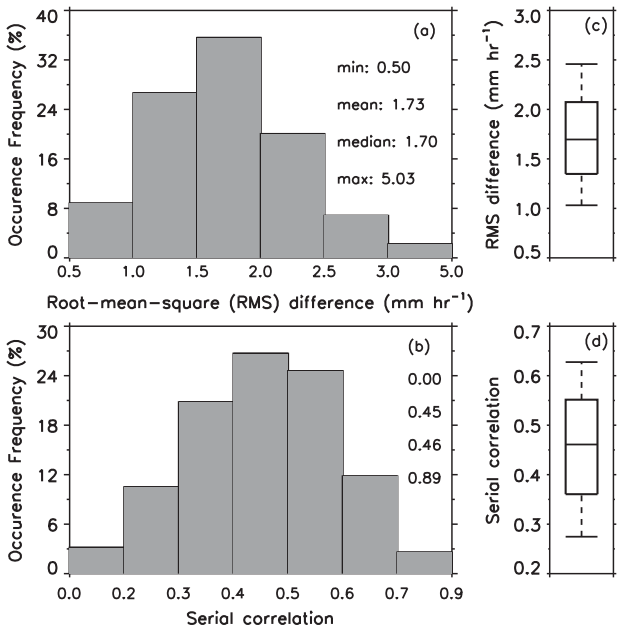

FIG. 13. Histograms of (a) RMS difference and (b) serial correlation between CMORPH and the rain gauge–based analysis over all grid boxes in the YHRB. Minimum, mean, median, and maximum values of the indicated variables are labeled from top to bottom in each panel. Box-and-whisker plots of (c) RMS difference and (d) serial correlation are also presented, showing the median (short line in the box), interquartile range (rectangle), and outliers (i.e., the 10th and 90th percentile as whiskers) for the indicated variables.

with the major peak rate (i.e., at 10.1 mm day^{-1}) taking place during the period of early morning hours [i.e., 0300–1000 local standard time (LST)] and the secondary peak rate (i.e., at 9.7 mm day^{-1}) in the afternoon hours (i.e., 1400–1800 LST). CMORPH depicts a bimodal pattern of the diurnal cycle of total precipitation rates with two minima occurring at about 1300 LST and 2300 LST, which is qualitatively in agreement with the rain gauge–based analysis. However, the CMORPH rainfall rates are substantially smaller during 0200–1500 LST, but larger during 1800–2400 LST, than those in the rain gauge–based analysis. As a result, the rain gauge–observed early morning rainfall peak is significantly underestimated, while the late afternoon peak is overestimated and delayed by 1–2 h. These results qualitatively agree with the findings of Shen et al. (2010, see their Figs. 12b,d).

As CMORPH's performance depends on the rain gauge–observed rainfall intensity (Fig. 9), diurnal cycles of the domain-averaged precipitation for the above-mentioned four rainfall categories are compared between CMORPH and the rain gauge–based analysis (Figs. 11b–e). Clearly, CMORPH underestimates the seasonal-mean rainfall amounts for the heavy and medium rainfall categories at each hour daily, although it captures the timings of peaks and troughs in their observed diurnal variations (Figs. 11b,c). On the other hand, CMORPH overestimates the seasonal-mean rainfall amounts for the light rainfall and clear sky categories at each hour daily (Figs. 11d,e). Of interest is that the CMORPH overestimations are the most (least) pronounced during 1800–2400 (0300–1200) LST, exceeding (being less than) the corresponding underestimations for the heavy and medium rainfall categories. Therefore, the CMORPH's overestimation of the late afternoon rainfall peak results from its significant overestimation for the light rainfall and clear sky categories.

Spatial distributions of the rainfall's diurnal variation is further examined (Fig. 12). The results suggest that the double-peaked diurnal cycle of the domain-averaged precipitation is a result of the averaging of different phases. During the early morning hours, the rainfall distribution resembles that of the total rainfall accumulation (Fig. 8a), that is, an elongated rainband located over the Huai River basin. In contrast, during the late afternoon hours, multiple rainfall centers are scattered over the area to the south of the early morning rainband. Relative to the rainstorms producing the early morning rainband, rainstorms producing these scattered rainfall centers tend to be of smaller spatial scale and shorter duration, as suggested by visual examination of the mosaic radar reflectivity on 3-km altitude at 6-min temporal intervals. This scale difference of rainstorms/rainfall events between the early morning and late afternoon hours over central-eastern China was also noticed by previous studies (e.g., Yu et al. 2007; Chen et al. 2010). One may conclude that CMORPH tends to overestimate rainfall (for the light rainfall and clear sky categories) when there are clouds associated with the smaller-scale rainstorms. Further study is needed to unravel the reasons for the dependence of the CMORPH's performance on the different rainfall categories.

c. *Temporal variation of precipitation*

To examine temporal variations of the hourly precipitation over all grid boxes from CMORPH against those from the rain gauge–based analysis, RMS difference and serial correlation are calculated for each grid box. Statistics of these parameters over all grid boxes are shown in Figs. 13a–d. A histogram of the RMS differences presents a single mode of 36% at 1.5–2.0 mm h^{-1}, with only 2% of them being larger than 3.0 mm h^{-1}. The median and mean values are 1.70 and 1.73 mm h^{-1}, respectively. Histogram of the correlation peaks at 0.4–0.5, with about 40% of them being larger than 0.5. The mean, median, and maximum values of correlation are 0.45, 0.46, and 0.89, respectively. Compared to the results of

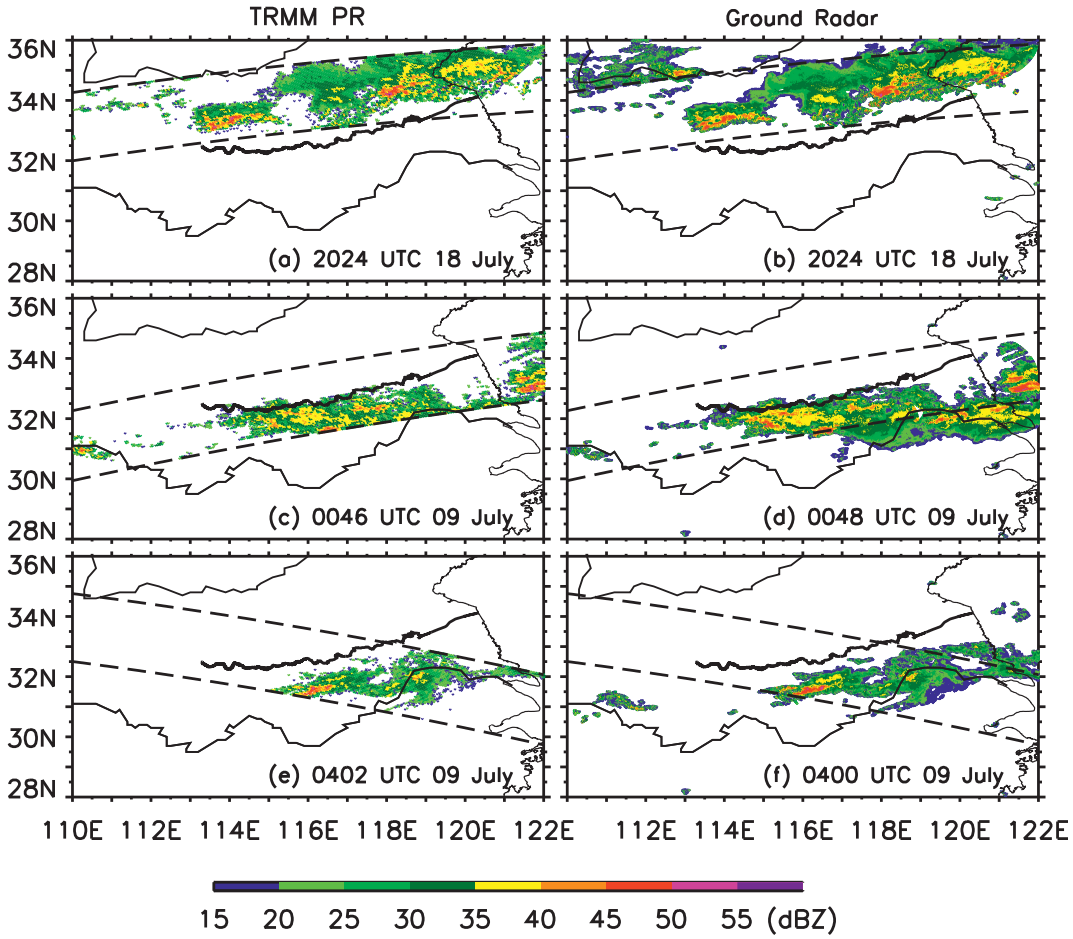

FIG. 14. Longitude–latitude distributions of radar reflectivity at 3-km altitude from (a),(c),(e) the TRMM precipitation radar observations and (b),(d),(f) the mosaic reflectivity data at approximately 2024 UTC 18 Jul, 0046 UTC 09 Jul, and 0402 UTC 09 Jul 2007, respectively. The dashed lines represent the boundaries of the TRMM satellite's pathway at the surface. The thick solid lines represent the Yangtze, Huai, and Yellow Rivers, while the thin solid lines represent the coastal lines.

Shen et al. (2010, see their Fig. 8c for the RMS difference and their Figs. 6b and 7b for the serial correlation), our study shows larger RMS differences and smaller correlations, mainly because the performance of satellite precipitation products improves as the averaging scale increases.

6. Summary and concluding remarks

In this paper, we have described procedures in the construction of a 8-km-resolution, gridded, hourly rainfall analysis dataset that is based on reports at 7127 AWSs over the YHRB region during the 2007 mei-yu season. This gridded analysis is obtained by a modified Cressman-type of objective analysis, following strict quality control, including careful verifications against mosaic radar reflectivity as well as internal consistency and extreme value checks. Hour-by-hourly comprehensive quantitative and qualitative assessments indicate that the gridded analysis can be used to study reasonably well many precipitation features, such as isolated thunderstorms, convective rainbands, leading convective lines followed by trailing stratiform rainfall, as well as mesoβ-scale rainfall extremes.

This rain gauge–based gridded hourly precipitation analysis is used to evaluate the CMORPH's performance at its original spatial resolution. Results suggest the dependence of the CMORPH's performance on the rain gauge–observed rainfall categories. Namely, the CMORPH tends to underestimate hourly rainfall rates over individual grid boxes on 8-km resolution when the rain gauge observations indicate occurrences of intense rainfall ($>5\,\mathrm{mm\,h^{-1}}$ in general and $>10\,\mathrm{mm\,h^{-1}}$ in particular) but overestimate it for the rain gauge–observed light rainfall and clear sky categories. While the underestimation presents insignificant diurnal variations,

the overestimation is more pronounced during the late afternoon and early evening hours (when rainstorms are of smaller scales) than the early morning hours (when rainstorms are of larger scale and longer duration). As a result, the major rainband and the early morning peak of the mei-yu precipitation are significantly underestimated, while the late afternoon peak is slightly overestimated by the CMORPH compared to the rain gauge observations.

In the present study, we have used this high-quality gridded rainfall analysis to help understand some spatial and temporal rainfall structures during the 2007 mei-yu season and reveal the dependence of the CMORPH's performance on the four different rainfall categories. Several journal articles will be forthcoming, showing detailed case studies of heavy rainfall events occurring during the 2007 mei-yu season using this dataset in conjunction with cloud-resolving simulations. We believe that this gridded analysis will be extremely valuable for evaluating the kilometer-scale-resolution, cloud-resolving simulations of MCSs and the performance of convective parameterization schemes in NWP and regional climate models. This analysis dataset will also be useful for many hydrometeorological applications.

Acknowledgments. This project was jointly funded by the National Basic Research Program of China (973 Program; 2012CB417202), the National Key Technology R&D Program of China (2012BAC22B03), the National Natural Science Foundation of China (Projects 41175049 and 41221064), and the Basic Research Fund of the Chinese Academy of Meteorological Sciences (CAMS 2012Y001). The authors acknowledge the anonymous referees for their valuable comments that have greatly improved the quality of this paper. Thanks also go to Drs. Shaorong Wu and Pingping Xie at NOAA/Climate Prediction Center for kindly providing the MWCOMB data.

APPENDIX

The Mosaic Reflectivity Data

The three-dimensional (3D) mosaic reflectivity data used in the present study is generated by applying the 3D multiradar mosaic software system developed by the State Key Laboratory of Severe Weather at the Chinese Academy of Meteorological Sciences (Wang et al. 2009). Inputs to the system are reflectivity measurements from 29 weather radars over the YHRB (see Fig. 1a for locations). The radars have many features similar to those of the Weather Surveillance Radar-1988 Doppler (WSR-88D) units used in the United States, that is, they are powerful 10-cm-wavelength radars with approximately 1° beam width by 1-km range resolution and volume scan sampling frequency of approximately 6 min. With an effective scan radius of about 150 km, the radar network could cover almost completely the YHRB region. Resolution of the 3D mosaic reflectivity data is 0.01° in the horizontal, and it varies in the vertical: 0.5 km below 6-km altitude and 1 km at 6–20-km height range. Comparisons with the coincident attenuation-corrected reflectivity (Iguchi et al. 2000) from the Tropical Rainfall Measuring Mission (TRMM; Simpson et al. 1996) precipitation radar observations (Kummerow et al. 2000) suggest high quality of the mosaic reflectivity data, especially at the altitudes of 2.5–4.5 km. Figure 14 provides three examples of the reflectivity distribution at 3-km altitude associated with mei-yu–frontal rainfall during this study period. It clearly indicates close agreement between the two data sources, which has also been confirmed by quantitative comparisons of the histograms of reflectivity (not shown). Because of the high resolution and large spatial coverage, the 3D mosaic reflectivity data is very valuable in revealing finescale rainfall structures of MCSs in the YHRB (e.g., Luo et al. 2010).

REFERENCES

Chen, H.-M., R.-C. Yu, J. Li, W.-H. Yuan, and T.-J. Zhou, 2010: Why nocturnal long-duration rainfall presents an eastward-delayed diurnal phase of rainfall down the Yantze river valley. *J. Climate,* **23,** 905–917.

Chen, M., W. Shi, P. Xie, V. B. S. Silva, V. E. Kousky, R. Wayne Higgins, and J. E. Janowiak, 2008: Assessing objective techniques for gauge-based analyses of global daily precipitation. *J. Geophys. Res.,* **113,** D04110, doi:10.1029/2007JD009132.

Cressman, G. P., 1959: An operational objective analysis system. *Mon. Wea. Rev.,* **87,** 367–374.

Ding, Y.-H., 1992: Summer monsoon rainfall in China. *J. Meteor. Soc. Japan,* **70,** 373–396.

——, and J. C. L. Chan, 2005: The East Asian summer monsoon: An overview. *Meteor. Atmos. Phys.,* **89,** 117–142.

Hu, J.-L., R.-H. Zhang, and T. Niu, 2008: A daily precipitation grid dataset with 0.1° resolution in Changjiang River valley and its precision (in Chinese with English abstract). *J. Nat. Resour.,* **23,** 136–149.

Iguchi, T., T. Kozu, R. Meneghin, J. Awaka, and K. Okamoto, 2000: Rain-profiling algorithm for the TRMM precipitation radar. *J. Appl. Meteor.,* **39,** 2038–2052.

Joyce, R. J., J. E. Janowiak, P. A. Arkin, and P. Xie, 2004: CMORPH: A method that produces global precipitation estimates from passive microwave and infrared data at high spatial and temporal resolution. *J. Hydrometeor.,* **5,** 487–503.

Kummerow, C., and Coauthors, 2000: The status of Tropical Rainfall Measuring Mission (TRMM) after two years in orbit. *J. Appl. Meteor.,* **39,** 1965–1982.

Luo, Y.-L., Y.-J. Wang, H.-Y. Wang, Y.-J. Zheng, and H. Morrison, 2010: Modeling convective-stratiform precipitation processes

on a Mei-Yu front with the Weather Research and Forecasting model: Comparison with observations and sensitivity to cloud microphysics parameterizations. *J. Geophys. Res.,* **115,** D18117, doi:10.1029/2010JD013873.

——, H. Wang, R.-H. Zhang, W.-M. Qian, and Z.-Z. Luo, 2013: Comparison of rainfall characteristics and convective properties of monsoon precipitation systems over South China and Yangtze and Huai River basin. *J. Climate,* **26,** 110–132.

Ni, Y.-Q., and X.-J. Zhou, 2006: Main scientific issues and achievements of State 973 project on study for formation mechanism and prediction theories of severe weather disasters in China (in Chinese with English abstract). *Adv. Earth Sci.,* **21,** 881–894.

Pan, Y., Y. Shen, Q.-Q. Yu, and P. Zhao, 2012: Merged analyses of gauge-satellite hourly precipitation over China based on OI technique (in Chinese with English abstract). *Acta Meteor. Sin.,* **70,** 1381–1389.

Ren, Z. H., and Coauthors, 2010: Quality control procedures for hourly precipitation data from automatic weather stations in China (in Chinese with English abstract). *Meteor. Mon.,* **36,** 120–132.

Shen, Y., A. Xiong, Y. Wang, and P. Xie, 2010: Performance of high-resolution satellite precipitation products over China. *J. Geophys. Res.,* **115,** D02114, doi:10.1029/2009JD012097.

Shepard, D., 1986: A two-dimensional interpolation function for irregularly-spaced data. *Proc. 1968 23rd ACM National Conf.,* Association for Computing Machinery, 517–524.

Simpson, J., C. Kummerow, W.-K. Tao, and R. F. Adler, 1996: On the Tropical Rainfall Measuring Mission (TRMM). *Meteor. Atmos. Phys.,* **60,** 19–36.

Tao, S.-Y., J. Wei, and X.-L. Zhang, 2008: Large-scale features of the Mei-Yu front associated with heavy rainfall in 2007 (in Chinese with English abstract). *Meteor. Mon.,* **34** (4), 3–15.

Ueda, H., and T. Yasunari, 1996: Maturing process of summer monsoon over the western North Pacific: A coupled ocean/atmosphere system. *J. Meteor. Soc. Japan,* **74,** 493–508.

Wang, H. Y., L. P. Liu, G. L. Wang, and Coauthors, 2009: Development and application of the Doppler weather radar 3-D digital mosaic system (in Chinese with English abstract). *J. Appl. Meteor. Sci.,* **20,** 214–224.

Xie, P., A. Yatagai, M. Chen, T. Hayasaka, Y. Fukushima, C. Liu, and S. Yang, 2007: A gauge-based analysis of daily precipitation over East Asia. *J. Hydrometeor.,* **8,** 607–626.

Yu, R., Y. Xu, T. Zhou, and J. Li, 2007: Relation between rainfall duration and diurnal variation in the warm season over central eastern China. *Geophys. Res. Lett.,* **34,** L13703, doi:10.1029/2007GL030315.

Zhang, H.-J., Q.-Y. Ma, H.-P. Wu, B. Luo, and W. Tang, 2009: Research on the interpolation algorithm for meteorological precipitation choroplethic map (in Chinese with English abstract). *Meteor. Mon.,* **35** (11), 131–136.

Zhang, M., and D.-L. Zhang, 2012: Subkilometer simulation of a torrential-rain-producing mesoscale convective system in east China. Part I: Model verification and convective organization. *Mon. Wea. Rev.,* **140,** 184–201.

Zhao, S.-X., L.-S. Zhang, and J.-H. Sun, 2007: Study of heavy rainfall and related mesoscale systems causing severe flood in Huaihe river basin during the summer of 2007 (in Chinese with English abstract). *Climatic Environ. Res.,* **12,** 713–727.